analytical chemistry

Article

pubs.acs.org/ac

Duplex Microfluidic SERS Detection of Pathogen Antigens with Nanoyeast Single-Chain Variable Fragments

Yuling Wang,[†,§] Sakandar Rauf,[†] Yadveer S. Grewal,[†] Lauren J. Spadafora,[⊥] Muhammad J. A. Shiddiky,[†] Gerard A. Cangelosi,[⊥] Sebastian Schlücker,*[,§] and Matt Trau*[,†,‡]

[†]Centre for Biomarker Research and Development, Australian Institute for Bioengineering and Nanotechnology (AIBN) and [‡]School of Chemistry and Molecular Biosciences, The University of Queensland, Brisbane, Queensland 4072, Australia

[§]Faculty of Chemistry, University of Duisburg-Essen, Essen, D-45141, Germany

[⊥]School for Public Health, University of Washington, Seattle, Washington 98195, United States

Supporting Information

ABSTRACT: Quantitative and accurate detection of multiple biomarkers would allow for the rapid diagnosis and treatment of diseases induced by pathogens. Monoclonal antibodies are standard affinity reagents applied for biomarkers detection; however, their production is expensive and labor-intensive. Herein, we report on newly developed nanoyeast single-chain variable fragments (NYscFv) as an attractive alternative to monoclonal antibodies, which offers the unique advantage of a cost-effective production, stability in solution, and target-specificity. By combination of surface-enhanced Raman scattering (SERS) microspectroscopy using glass-coated, highly purified SERS nanoparticle clusters as labels, with a microfluidic device comprising multiple channels, a robust platform for the sensitive duplex detection of pathogen antigens has been developed. Highly sensitive detection for individual *Entamoeba histolytica* antigen EHI_115350 (limit of detection = 1 pg/mL, corresponding to 58.8 fM) and EHI_182030 (10 pg/mL, corresponding 453 fM) with high specificity has been achieved, employing the newly developed corresponding NYscFv as probe in combination with SERS microspectroscopy at a single laser excitation wavelength. Our first report on SERS-based immunoassays using the novel NYscFv affinity reagent demonstrates the flexibility of NYscFv fragments as viable alternatives to monoclonal antibodies in a range of bioassay platforms and paves the way for further applications.

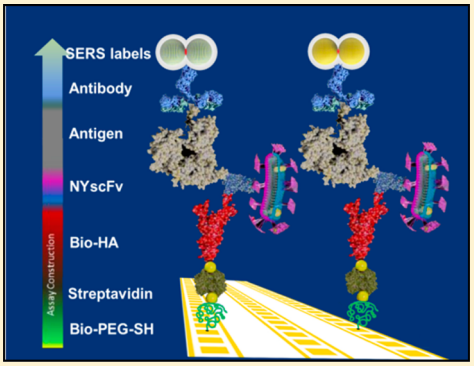

Protein biomarkers are widely used as targets for disease diagnostics, which allow the identification of species at a molecular level. Monoclonal antibodies (mAbs) are the current gold standard affinity reagents used for protein biomarker (antigen) detection. However, highly specific mAbs are expensive and time-consuming to isolate and manufacture. Alternative affinity reagents have been developed in part to address these issues,[1,2] but they often have limitations of their own, such as lack of specificity or stability, that have prevented their further development into diagnostic practice. For example, single-chain variable fragments (scFv) are affinity reagents that can be inexpensively and quickly selected from libraries displayed on yeast, phage, or bacteria.[2−5] Yeast-displayed scFv are selected by fluorescence-activated cell sorting (FACS) for affinity and stability when bound via Aga1−Aga2 linkages to yeast cell walls. Unfortunately, scFv, which have excellent activity on yeast surfaces, often lose their activity once in solution, an environment for which they were not selected. To address these limitations, we previously developed nanoyeast-scFv (NYscFv) affinity reagents, which were enriched by binding to surface-attached antibodies specific to the scFv's epitope tags.[6,7] Further, these NYscFv fragments have been developed as a replacement for monoclonal antibodies in our previous work[7,8] by applying electrochemical methods for sensitive detection of recombinant *Entamoeba histolytica* (*E. histolytica*), which is a prevalent waterborne pathogen that infects humans, causing invasive intestinal and extraintestinal diseases, and is estimated to cause 50 million infections worldwide and up to 100 000 deaths annually in developing countries.[9,10] Conventional molecular tests for *E. histolytica* antigen detection include enzyme-linked immunosorbent assay (ELISA) and fluorescence-based approaches, in which monoclonal antibodies are the current gold standard affinity reagents used for antigen detection. However, the demands of rapid diagnosis and treatment of disease induced by pathogens require a robust platform that could utilize the low-cost, stable and highly specific NYscFv as the affinity reagent for sensitive and accurate multiplexed detection of pathogen antigens.

Surface-enhanced Raman scattering (SERS) is an emerging readout technique that can selectively and sensitively detect biomolecules, such as peptides, proteins and nucleic acids with

Received: July 21, 2014
Accepted: September 5, 2014
Published: September 5, 2014

   dx.doi.org/10.1021/ac5027012 | *Anal. Chem.* 2014, 86, 9930−9938

high sensitivity and chemical specificity, allowing multiplexed detection using only a single laser excitation wavelength.[11−15] Sensitivity and reproducibility of SERS-based assays are strongly dependent on the quality of the SERS nanoparticle labels in terms of signal strength and colloidal stability. A SERS nanoparticle label comprises of a noble metal nanoparticle coated with Raman reporter molecules for identification based on their characteristic vibrational Raman spectrum (or barcode representation). Generally, the SERS enhancement is attributed to the electromagnetic (EM) and chemical effect (CE), in which the EM contribution plays a dominant role for the overall enhancement. Typically, the EM enhancement is highest in a so-called "hot spot", which may be generated by excitation of a localized surface plasmon resonance (LSPR) in metal nanoparticles with very close distances. The generated large EM field leads to a significantly increased sensitivity down to the single-molecule level.[16−19] Although aggregated nanoparticles are often used for generating hot spots for obtaining high Raman signals, SERS signals are generally hard to reproduce and quantify since it is difficult to control the aggregation of the nanoparticles including their interparticle distance. Therefore, controlling the enhancement of Raman reporters on the surface of the nanostructures with reproducible signal has been of great importance for ultrasensitive and reproducible detection in bioassays. Although numerous efforts have been devoted to address this issue, the preparation of highly purified and sensitive SERS labels is still a challenge. We recently exploited an efficient approach to purify gold nanoparticles in the 20−250 nm size range by continuous density gradient centrifugation.[20] Overall, using highly purified, silica-encapsulated clusters of gold nanoparticles as SERS labels provides the following advantages: (i) the silica-coating makes the particles very stable in physiological environments (different buffers) and offers a versatile surface for bioconjugation,[21] (ii) a self-assembled monolayer (SAM) of Raman reporter molecules on the entire surface of the gold nanoparticles as well as in the hot spots formed in the junction between gold nanoparticles provides maximum sensitivity, and (iii) purification of the clusters contributes to a reproducible signal for the detection.

In this contribution, by employing the newly developed NYscFvs as alternative affinity reagents and silica-coated, highly purified SERS clusters as sensitive labels, we attempt to explore a powerful laboratory diagnostic platform that can sensitively and accurately provide duplex detection of target *E. histolytica* pathogen antigens simultaneously, with the help of a microfluidic device that contained multiple channels to facilitate the detection. Furthermore, this new SERS readout platform for NYscFvs reagents will confirm the utility and adaptability of nanoyeast-scFv as an alternative to monoclonal antibodies in a range of diagnostic platforms. The incorporation of inexpensive NYscFv reagents with SERS will also demonstrate a powerful analytical platform that could be potentially useful for high throughput multiplexed detection of pathogen antigens.[22]

EXPERIMENTAL SECTION

Chemicals and Materials. 4-Mercaptobenzoic acid (MBA), 5,5′-dithiobis(2-nitrobenzoic) (DTNB), tetraethoxyorthosilicate (TEOS), (3-aminopropyl)-trimethoxysilane (APTMS), ammonium hydroxide (30%), *N*′-(ethylcarbonimidoyl)-*N*,*N*-dimethyl-monohydrochloride (EDC), *N*-hydroxysulfosuccinimide sodium salt (s-NHS), and 4-(2-hydroxyethyl)-1-piperazineethanesulfonicac (HEPES), were purchased from Sigma-Aldrich/Fluka. 4-Mercapto-3-nitro benzoic acid (MNBA) was prepared by breaking the disulfide bond in DTNB with $NaBH_4$ as reducing agent before usage.

Monodispersed gold nanoparticles (AuNPs) with a diameter of around 55 nm were prepared via a modified seed-growth method reported by Perrault and Chan.[23]

Lyophilized yeast-scFv, and *E. histolytica* antigens EHI_115350, EHI_182030, and EHI_044550 (called "**350**", "**030**", and "**Jacob**" respectively) in this report were produced by The University of Washington, USA, and the Seattle Structural Genomics Center for Infectious Disease (SSGCID).[6,21−26] *Entamoeba histolytica* proteins EHI_115350 and EHI_182030 are *E. histolytica* cyst proteins. They are known to be present in cysts based on proteomic[27] or transcriptomic[28] analyses. Therefore, they are likely to be present in patient stool and thus are potential good biomarkers for *E. histolytica* infection. The purified antigens and selection of yeast scFv are previously described in Grewal et al.[7,8] Biotinylated anti-HA antibody was purchased from Sapphire Bioscience. SH-PEG-Biotin was purchased from Fisher Scientific. Streptavidin was procured from Invitrogen. Phosphate buffered saline (PBS) tablets were purchased from Astral Scientific.

The polyclonal rabbit anti-350 antisera were generated against recombinant antigen by Cocalico Biologicals, Inc., Reamstown, PA, USA.[9,26] Chicken IgY raised against a cocktail of 030 and three additional *Entamoeba histolytica* antigens (EHI_006810, EHI_070730, and EHI_101240) was prepared by Aves Laboratories, Tigard, OR, USA. Nonspecific IgY was subtracted against 4 consecutive aliquots of 2 billion yeast-cells prior to conjugation to the SERS nanoparticle clusters.

Preparation of Silica-Encapsulated, SAM-Coated Gold Nanoparticle Clusters. Colloidal gold nanoparticles (AuNPs, 600 mL) with a diameter of 55 nm (λ_{max} = 535 nm in water) were centrifuged and redispersed in 100 mL ethanol. The colloid was then incubated overnight with 9 mL of Raman reporter solutions (MNBA and MBA, 10 mM in ethanol) to form a complete self-assembled monolayer (SAM) on the particle surface. Aggregation of the nanoparticles was induced by adding few microliters of PBS buffer solution under stirring. After 30 min, the aggregated colloidal solution was centrifuged three times and washed in 50 mL of ethanol to remove the excess salts. Silica encapsulation of the SAM-coated aggregated colloids (AuNPs-MNBA and AuNPs-MBA) was performed using a previously reported method.[20] The thickness of the silica shell was adjusted by the amount of TEOS. After several hours of incubation, silica-coated SERS clusters were centrifuged to remove the incubation solution, and the precipitate was redispersed into ethanol.

Continuous Density Gradient Centrifugation. Purified SERS clusters including dimer and trimers were obtained by using continuous density gradient centrifugation.[20] Briefly, 50 mL of water/glycerol mixtures with different compositions (30, 35, 40, 45, and 50 vol % glycerol) were prepared. Two milliliters from each water/glycerol mixture were stacked on top of each other, starting with the 30% mixture at the bottom of the tube. After vertical stacking, the tube was carefully turned horizontally for the formation of a continuous density gradient within 5 min. Additionally, the tubes were centrifuged for 5 min. The colloidal mixtures were redispersed in 100 μL PVP/ethanol solution and stacked on top of the continuous density gradient. After centrifugation, the particles were extracted from

dx.doi.org/10.1021/ac5027012 | *Anal. Chem.* 2014, 86, 9930−9938

the tube with a hypodermic needle by injection through the wall of the plastic tube.

Biofunctionalization of Silica-Coated SERS Nanoparticle Clusters. Silica-coated SERS nanoparticle clusters were conjugated with antibodies after modification of the silica surface by a siliane agent and standard EDC chemistry.[29] Briefly, 1600 μL of SERS clusters (OD = 2.75) were first hydrolyzed with 268 μL ammonia (28%) under sonication at room temperature (RT) for 20 min. Afterward, the SERS clusters were centrifuged once and redispersed into ethanol. Sixty-eight microliters APTMS (0.5%) and 68 μL of ammonia were added to the activated SERS clusters and incubated at RT for 20 min under sonication. Amino-functionalized SERS clusters were further conjugated with 120 μL of succinic anhydride to form carboxyl groups on the cluster. SERS clusters were centrifuged at 7000 rpm for 10 min and then washed in HEPES twice. SERS clusters were redispersed into HEPES buffer and activated by EDC/s-NHS (5 mg/1.5 mL for EDC and 3.77 mg/1.5 mL for s-NHS). Two micrograms of polyclonal antibody was added to the SERS clusters and incubated at room temperature (25 °C) for 30 min and 4 °C overnight. SERS clusters were then centrifuged at 7000 rpm for 10 min at 4 °C and redispersed in 0.5% BSA-PBS buffer prior to use in the bioassay. The as-prepared SERS labels are very stable and can be stored for several days before use.

Fabrication of Multiplexed Microfluidic Platform. The multiplexed microfluidic device was fabricated using standard photolithography procedures and sandwiched between custom built holders to introduce inlets and outlets for the reagents. Briefly, the gold patterns of widths 25 and 125 μm with spacing 25 μm were fabricated on a glass wafer using photolithography. The gold patterns were designed in Layout Editor (L-Edit V15, Tanner Research Inc., CA) and printed on a chrome mask (5 in. × 5 in.) obtained from Qingyi Precision Mask-making (Shenzhen) Ltd., China. Pyrex glass wafers (4 in., 1 mm thick, double-side polished) were obtained from Bonda technology, Singapore. The glass wafers were first cleaned in acetone and isopropyl alcohol (IPA) by sonication for 5 min in each case, rinsed with IPA, and dried with nitrogen gas. These were then coated with a negative photoresist (AZ nLOF 2070) at 3000 rpm for 30 s to obtain ∼7 μm thick resist layer. The negative photoresist coated wafers then underwent a soft baking step at 110 °C for 6 min. These wafers were exposed to UV light (280 mJ/cm^2) using the mask aligner (EVG 620, EV Group GmbH, Austria), and, after a post exposure bake step at 110 °C for 3 min, they were developed in AZ 726 developer solution for 3 min, followed by rinsing with deionized (DI) water (Millipore Pvt. Ltd., Australia) and drying under the flow of nitrogen gas. In this step, the unexposed negative photoresist was removed to realize the photoresist pattern. The wafers were then treated with oxygen plasma (60 W for 45 s) to remove any residual resist layer. The gold deposition (10 nm of titanium as adhesion layer followed by 200 nm of gold layer) was carried out using a Temescal BJD-2000 E-beam evaporator. To obtain the gold patterns, these wafers were then immersed in ethanol for lift-off process. Finally, the wafers were diced into individual devices using the ADT-7100 dicing machine.

Each device was covered with polydimethylsiloxane (PDMS) containing three 400 μm wide and 25 mm long channels with 1 mm diameter inlets and outlets. The PDMS molds were made by casting from SU8−2150 (MicroChem, U.S.A) master fabricated on a silicon wafer by following the standard photolithography process as per manufacturer's instructions. Briefly, the PDMS precursor was mixed with curing agent (10:1) (Sylgard 184 kit, Dow Corning), and, after degassing, it was poured on top of the SU-8 master followed by curing at 65 °C for 4 h. After this, the PDMS was released from the master, and 1 mm-holes were punched into PDMS to open inlets and outlets.

Fabrication of the Assay. The bioassay platform was fabricated according to several steps. Briefly, gold coating glass chips with 3 channels were first cleaned with Piranha solution and connected with PDMS to separate each channel. Afterward, the device was fixed into the microfluidic platform. Biotin-PEG-SH at the concentration of 2−3 mg/mL in ethanol was injected into each channel and left for the reaction at room temperature overnight. After washing each channel several times using PBS buffer, 0.5 mg/mL streptavidin was reacted with biotin-PEG for 1 h. Bioanti-HA antibody was then employed to react with streptavidin at RT for 1 h, leading to the immobilization of the anti-HA antibody on the gold surface. The nanoyeast-scFv reagent diluted 1/10 in PBS was allowed to bind with anti-HA antibody for 1 h after washing with PBS.

The sensing gold surface was then incubated with antigen solution at varying concentrations for another hour. Finally, the sensor interface was incubated with the corresponding SERS labels to complete the immunoassay platform. Further work is in progress which aims at enhancing the binding kinetics between the biomolecules and nanoparticles by applying external forces (e.g., electric forces). This should reduce the assay time, which is a necessary requirement for real life applications.

Instruments. SERS clusters were characterized by transmission electron microscopy (TEM) (JEOL-2100) and UV−vis extinction spectroscopy (PerkinElmer, Lambda 35). Scanning electron microscopy (SEM) (Philips XL30) was applied to characterize and localize single particles on a silica wafer in single-particle experiments and to demonstrate the binding of SERS clusters on the gold surface at negative and positive conditions.

Electrochemical experiments were performed at room temperature (25 °C) using gold chip as working electrodes, Ag reference, and platinum as counter using an electrochemical analyzer CHI 650D (CH Instruments, Austin, TX). Electrochemical impedance spectra (EIS) were measured in a 10 mM phosphate buffer solution (pH 7.4) containing 2.5 mM $[Fe(CN)_6]^{3-}/[Fe(CN)_6]^{4-}$ (1:1) and 0.1 M KCl, using an alternating current voltage of 10 mV, with the frequency range of 1 Hz−100 kHz.

SERS spectra were recorded with a WITec alpha 300 R microspectrometer. The 632.8 nm line from a HeNe laser was used for excitation of Raman scattering. SERS images and spectra were obtained at 20 ms integration time with an EMCCD, mapping an area of 76 μm × 50 μm (100 pixel ×100 pixel) using a 20× microcopy objective (100× objective for single-particle SERS measurement). A silicon wafer was used for calibration of the system by checking the laser power and focusing conditions based on the Raman intensity of the first-order photon peak of silicon at ca. 520 cm^{-1}.

RESULTS AND DISCUSSION

Silica-Coated, Highly Purified SERS Nanoparticle Clusters with Spectral Multiplexing Capability and Single-Particle Sensitivity. Highly purified, silica-coated SERS nanoparticle clusters were prepared based on the chemisorption of Raman reporters on gold nanoparticles

dx.doi.org/10.1021/ac5027012 | Anal. Chem. 2014, 86, 9930−9938

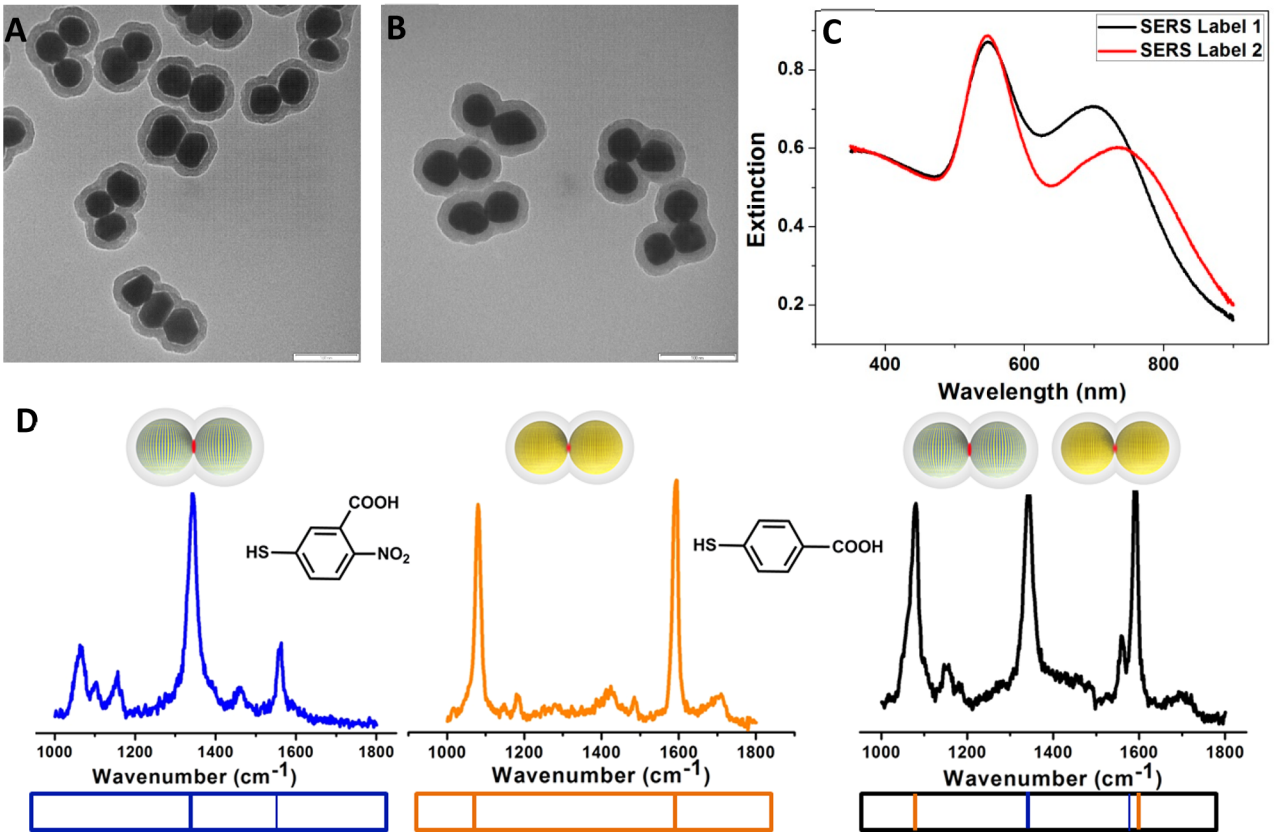

Figure 1. TEM images of silica-coated, highly purified SERS nanoparticle clusters with Raman reporters 1-MNBA (A) and 2-MBA (B). Extinction spectra (C) and SERS spectra (D) of the nanoparticle clusters including a binary mixture.

(AuNPs) forming a self-assembled monolayer (SAM) on the metal surface. Particle aggregation was induced by salt, followed by coating with silica (Stöber synthesis) and continuous density gradient separation as described in the Experimental Section (Supporting Information Figure S1). The formation of a SAM provides maximum coverage of the AuNPs surface with Raman reporters in order to generate maximum Raman signals and minimize coadsorption of other molecules.[30,31] In this study, 4-mercapto-3-nitro benzoic acid (MNBA) and 4-mercaptobenzoic acid (MBA), both small aromatic thiols, were used as the Raman reporters, exhibiting only few dominant Raman bands for identification.[30] The as-prepared SERS nanoparticle clusters were first characterized by TEM (Figures 1A and 1B). High-purity yields of silica-coated SERS nanoparticle dimers and trimers (shell thickness around 15 nm) were generated using MNBA (Figure 1A) and MBA (Figure 1B) as Raman reporters, respectively, and no monomers or large aggregates were observed.

A typical high resolution TEM image further demonstrates that the gap between the dimers was around 1−2 nm (Supporting Information Figure S2), which will generate a strong EM field for SERS enhancement (hot spot).[16,17] Optical properties of the SERS labels were investigated by extinction spectroscopy as depicted in Figure 1C, in which the first peak located at 535 nm from both SERS labels is attributed to the characteristic dipolar localized plasmon resonance of 55 nm AuNPs. Additional plasmon peaks at higher wavelengths (located at 690 and 735 nm for MNBA and MBA, respectively) are also observed, which correspond to additional plasmon modes arising from plasmonic coupling between closely spaced AuNPs.

Figure 1D shows the molecular structure of the Raman reporters applied in this study together with their corresponding SERS spectra including a simplified barcode representation (both single "colors" as well as a binary mixture). The characteristic Raman peak of MNBA at 1340 cm^{-1} is assigned to the symmetric nitro stretching vibration,[11] while the peaks at ca. 1080 and ∼1580 cm^{-1} for MNBA and MBA arise from phenyl ring modes.[32] The SERS spectrum of the binary mixture (MNBA and MBA) clearly shows the distinct fingerprints from the corresponding SERS labels, demonstrating the duplex capability of this approach.

The signal brightness of the as-prepared SERS labels was investigated by collecting SERS signals from single particles, which provides the most direct and unambiguous way for establishing structure−activity correlations.[33] SEM images were used to characterize a single SERS particle on a silicon wafer patterned with gold-framed squares and numbers, which enabled the fast identification/localization of exactly the same particle under the optical/Raman microscope (Supporting Information Figure S3). False-color SERS images from single particles were obtained by choosing a Raman point-mapping acquisition scheme with EMCCD detection and an integration time of 30 ms per pixel.[34] In the SERS false-color images, bright dots were observed from the chosen mapping area (red-square), and the corresponding SERS spectra obtained from the bright dots indicated the distinct peak of MNBA at 1340 cm^{-1} (Supporting Information Figure S3A, corresponding to the symmetric nitro stretching vibration of MNBA,[11]) and of MBA at 1580 cm^{-1} (Supporting Information Figure S3B, corresponding to the phenyl ring modes of MBA[32]), demonstrating the single-particle sensitivity of the SERS labels

dx.doi.org/10.1021/ac5027012 | Anal. Chem. 2014, 86, 9930−9938

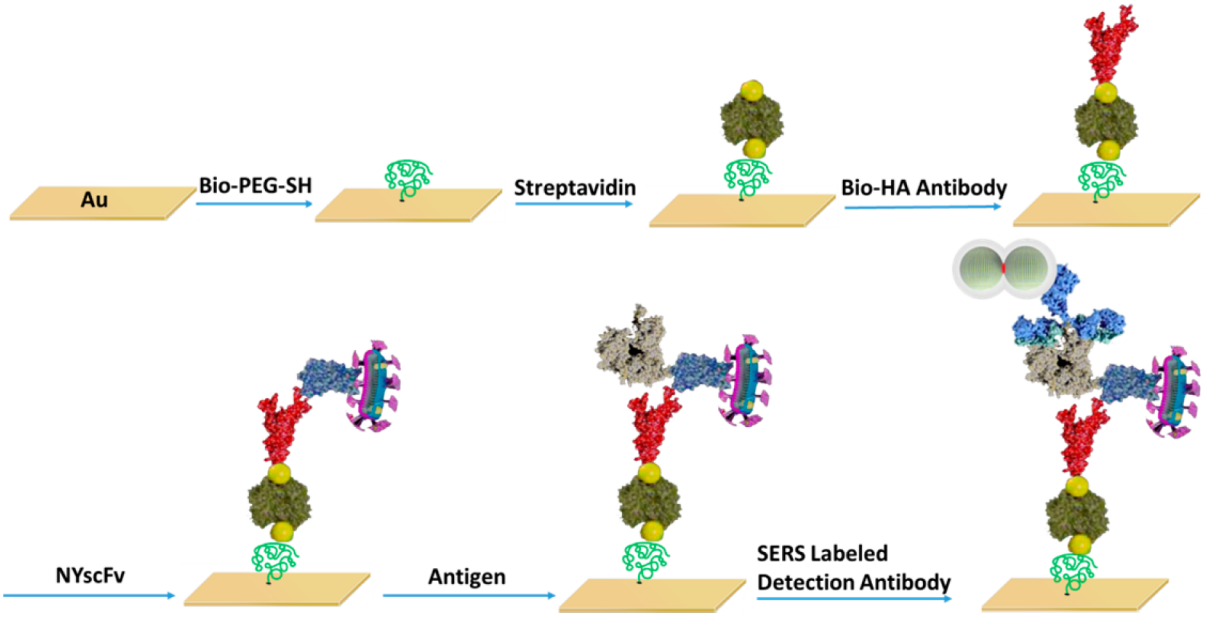

Figure 2. Schematic illustration for constructing a SERS-based assay utilizing NYscFv fragment as probe for pathogen antigen detection (not drawn to scale).

employed in this work, which is the basis for the high sensitivity of the duplex assay.

Principle of the SERS Bioassay. Figure 2 depicts the principle of the SERS bioassay platform for pathogen antigen detection coupled with nanoyeast-scFv (NYscFv) as the affinity reagent on the gold substrate. Briefly, thiolated-PEG-biotin was conjugated to the gold surface. Multivalent streptavidin was applied to link a biotinylated antihuman influenza hemagglutinin tag antibody (biotin-HA antibody), which captures the NYscFv by virtue of an HA antigen tag cloned into the recombinant scFv construct. The assembly of the different biomaterial layers was monitored by electrochemical impedance spectroscopy (EIS), which is an efficient technique to probe the buildup of the biomaterial sensing film and monitor the change on the electrode surface through the electron-transfer resistance (as indicated in Supporting Information Figure S4).[7,8] With the binding of different layers, the electron-transfer resistance (R_{ct}) increased, indicating successful stepwise binding of biomolecules on the gold surface. The bound NYscFv was then employed for capturing the target *E. histolytica* protein EHI_115350, called **350** or EHI_182030, called **030** depending on the type of NYscFv applied.

Once the target antigen was captured, SERS labels conjugated to antigen-specific polyclonal antibodies were adsorbed on the surface to produce the specific barcode for the antigen detection. The bioconjugation of SERS nanoparticle clusters to antibodies was based on the modification of the silica surface by the silane reagent and the cross-linker as illustrated in Figure S5 (Supporting Information). SERS label-1 was conjugated to a 1:10 dilution of unpurified, monospecific rabbit α-350 sera, whereas SERS label-2 was attached to unpurified, polyspecific chicken IgY that had been raised against **030** and three other *Entamoeba* antigens. Depending on the concentration of the antigen, different amount of SERS labels are expected to attach to the gold chip surface due to the strong affinity between the antigen and the antibody, generating different levels of SERS signal corresponding to different concentrations for readout.

Sensitive Detection of Individual Pathogen Antigens (350 and 030). Sensitive pathogen antigen detection was conducted with our previously developed, spatially resolved microspectroscopic SERS detection scheme using confocal Raman point mapping.[35,36] It should be noted that this scheme significantly improves the statistical reproducibility and countervails spot-to-spot variation in conventional SERS assays with single-spot readout. Figure 3A shows typical false-color SERS images using the integrated Raman intensity of the MNBA marker band between 1330 to 1360 cm^{-1} in an area of 76 μm × 50 μm (100 pixels ×100 pixels = 10 000 pixels). Upon increasing the concentration of antigen **350**, more and more SERS labels were captured on the gold chip surface and consequently generated brighter SERS images. To test the reproducibility of this assay, repeated experiments were conducted on three different days and performed on five different gold chips during the same day. The results are summarized in Figure 3, in which individual SERS spectra were obtained, averaged, and analyzed, demonstrating distinct peaks from the corresponding SERS labels and brighter intensities with increasing antigen concentration. The concentration-dependent SERS response in Figure 3C is based on the average SERS spectra intensity of the Raman reporter's nitro band at 1340 cm^{-1} obtained at antigen concentrations from 0 pg/mL to 10 ng/mL. The lowest detectable concentration for **350** was determined to be ~1 pg/mL (58.8 fM) (Figure 3), for which the signal is three-times higher than the noise (for 0 pg/mL) as well as with the detection of **350** at 0.1 pg/mL, which was found to be similar to that of the background (Supporting Information Figure S6). The linearity (R^2 = 0.96) is seen more clearly in Supporting Information Figure S6, which shows the 0−10 ng/mL range on a linear concentration scale, along with the linear regression line.

To clearly demonstrate the specific detection of *E. histolytica* pathogen antigen by this NYscFv-SERS platform, negative control experiments were also performed at different conditions: (i) without NYscFv fragment, (ii) without antigen, and also with (iii) a noncognate antigen (**Jacob**) at a

dx.doi.org/10.1021/ac5027012 | *Anal. Chem.* 2014, 86, 9930−9938

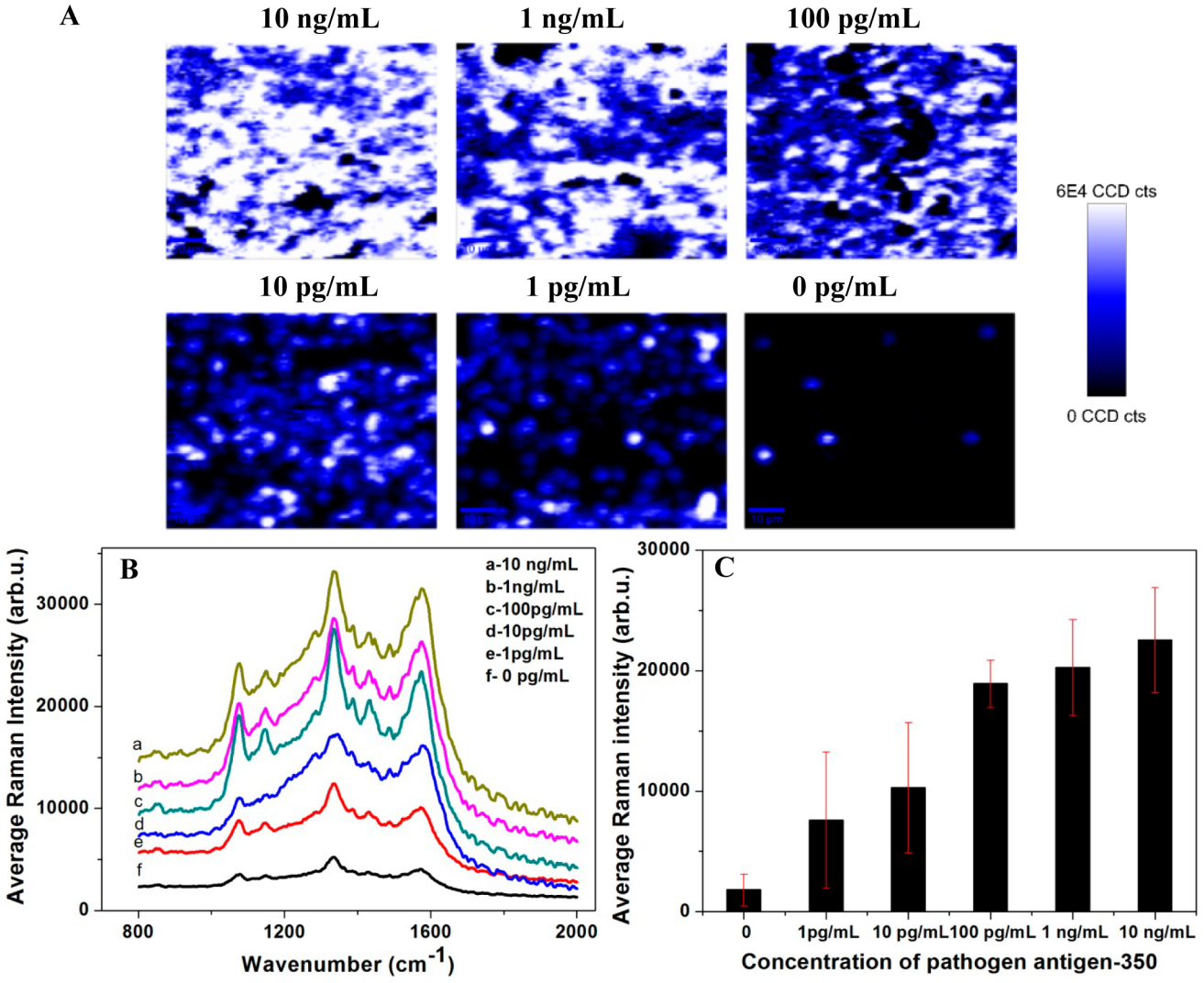

Figure 3. False-color SERS images for the detection of **350** at different concentrations (A), corresponding average SERS spectra obtained from confocal SERS mapping data sets (B), and concentration-dependent average SERS intensity for detection of **350** (C).

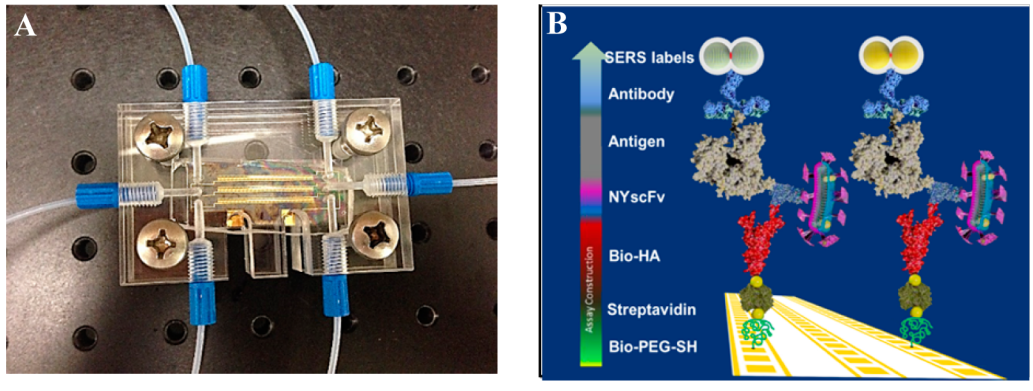

Figure 4. Photograph of the 3-channel microfluidic device containing gold patterns (A) and schematic illustration of the SERS biosensor platform with NYscFv for duplex antigen detection (B).

concentration of 1 μg/mL as indicated in Supporting Information Figure S7. Only very weak SERS signals were detected in these negative controls. For comparison, the SERS intensity was much stronger for the target (**350**), even at a low concentration of 1 ng/mL. As an additional SEM images were further used to visualize the gold surface based on specific binding of NYscFv with the target antigen and the SERS labels (Supporting Information Figure S7B and C). Silica-coated SERS nanoparticle clusters were observed only when the target molecule was employed (Supporting Information Figure S7C), while a very clean surface was found in case of the negative

dx.doi.org/10.1021/ac5027012 | *Anal. Chem.* 2014, 86, 9930−9938

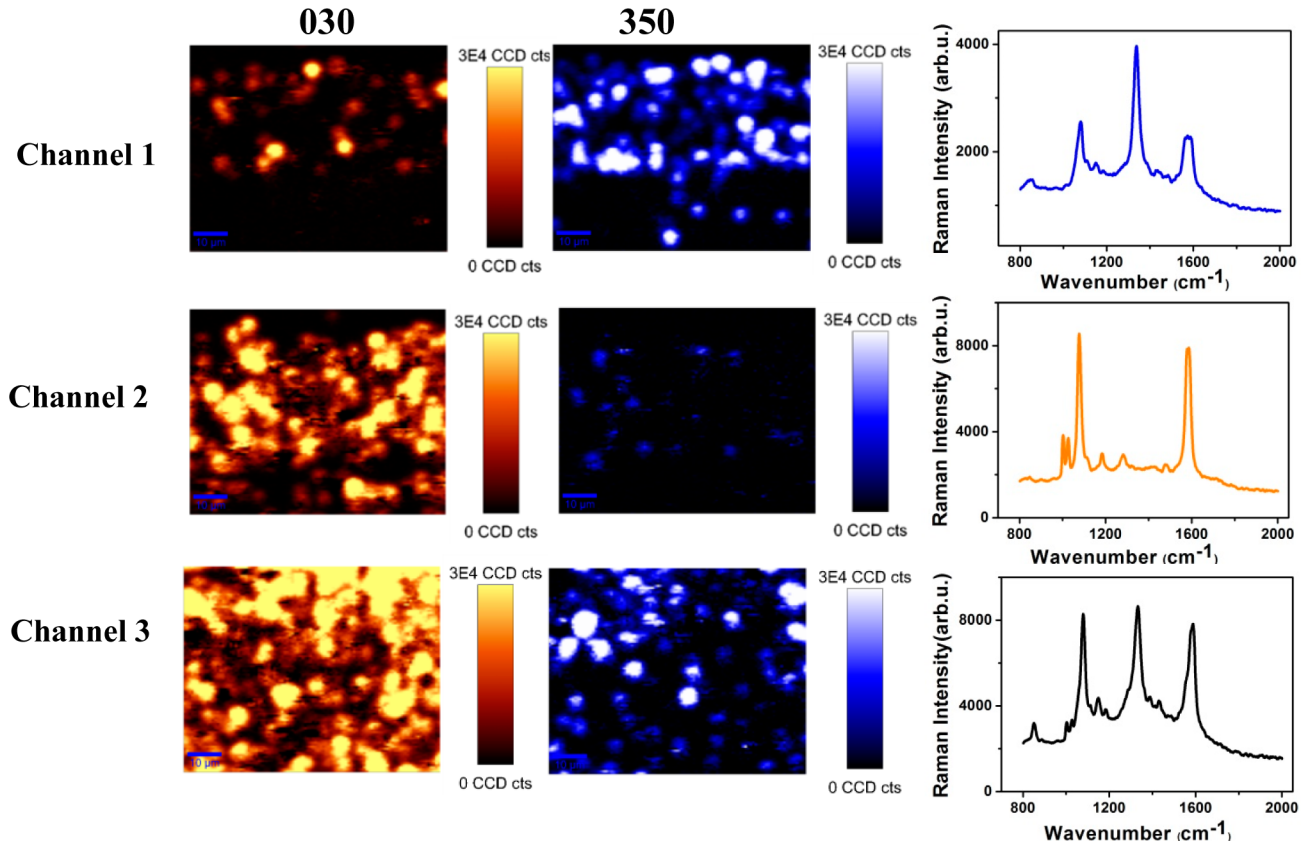

Figure 5. False-color SERS images and the corresponding average SERS spectra for the duplex detection of pathogen antigens (**350** at 500 pg/mL and **030** at 5 ng/mL) in the 3-channel microfluidic device.

control (Supporting Information Figure S7B), further demonstrating the specificity of this assay.

SERS for the detection of the second antigen (**030**) was performed at the same optimized condition as for the first one (**350**). As shown in Figure S8 A (Supporting Information), the brightness in the false-color SERS images increases with the concentration of **030** antigen, again demonstrating that the SERS labels are specifically captured onto the gold surface. This is also reflected in the corresponding average SERS spectra (Supporting Information Figure S8B). Finally, the lowest detectable concentration for **030** was determined to be 10 pg/mL (453 fM) with high specificity (Supporting Information Figure S8C). Notably, the lowest detectable concentration for **350** and **030** detection was a 10-fold difference, which is most likely due to the different binding affinities between the SERS label-conjugated polyclonal antibodies and their target antigens. In similar ELISA and flow cytometric assays, the α-350 rabbit sera has demonstrated lower optimal titers with yeast-scFv when compared to the α-030 chicken antibody (data not shown).

Microfluidic Device for Duplex Detection of Pathogen Antigens. A microfluidic device with multiple channels was developed for the duplex detection of pathogen antigens as illustrated in the photograph and scheme in Figure 4. Microfluidic channels were connected with three inlets and three outlets to enable the detection of multiple targets simultaneously. Each channel contained gold patterns which can be used for the functionalization of the device using gold–thiol chemistry. The detailed design and fabrication for this device is shown in Figure S9 (Supporting Information). In this proof-of-concept study, this newly developed microfluidic device was employed for the duplex detection of pathogen antigens.

As displayed in Figure 4B, duplex antigen detection was performed on the three channels simultaneously. Specifically, NYscFv-**350** was immobilized on the gold surface in the first channel. And NYscFv-**030** was bound on the surface in the second channel. In the third channel, both scFv-**030** and **350** (at the ratio of 1:1) were immobilized to capture both antigens. After immobilization, all the three channels were incubated with the antigens **350** and **030** (500 pg/mL and 5 ng/mL, respectively) and the two different SERS labels. It should be noted that two antigens at different concentrations were employed because of the different detection sensitivities for **350** and **030** (1 vs 10 pg/mL) as discussed above.

Figure 5 shows false-color SERS images and the corresponding average SERS spectrum for the duplex antigen detection. Typically, in the first channel, dominant signals from **350**-specific SERS label-1 were obtained, with some cross-reaction 030 by SERS label-2. Moreover, in the second channel, false-color SERS images and the average SERS spectrum generated by dominant SERS label-2 demonstrated the specific detection for **030**, also with weaker cross-reaction by SERS label-1. Cross-reactive signals were likely because of the 10-fold excess of noncognate **030** antigen being applied to the channel, with limited cross reactions observed at lower concentrations of **030** antigen (data not shown). Weaker cross-reactive signals may be due to the crude polyclonal antibodies interacting nonspecifically with platform components, especially with yeast-scFv, as seen in other assays (data not shown). Furthermore, SERS images and the average SERS spectrum (distinct peaks at 1340 and 1580 cm^{-1} with a ratio intensity of 1:1) from the third

dx.doi.org/10.1021/ac5027012 | *Anal. Chem.* 2014, 86, 9930–9938

channel clearly demonstrated the simultaneous detection of the two pathogen antigens.

CONCLUSIONS

In summary, we have demonstrated a robust and sensitive SERS-based bioassay platform for simultaneous and sensitive detection of two pathogen antigens utilizing nanoyeast-scFv as a cost-effective, stable and specific affinity reagent. Silica-coated, highly purified SERS nanoparticle clusters were employed for readout, enabling the sensitive duplex detection of antigens. The microfluidic device with multiple channels enables a rapid and accurate detection of antigens. Finally, ultrasensitive and specific detection for individual **350** and **030** was achieved with limits of detection of ~1 (58.8 fM) and 10 pg/mL (453 fM), respectively. The demonstrated duplex detection of **350** and **030** paves the way for a powerful analytical platform that could be potentially useful for high throughput multiplexed detection of biomarkers.

ASSOCIATED CONTENT

Supporting Information

Schematic illustration for preparing silica-coated, highly purified SERS nanoparticle clusters; a high-resolution TEM image of SERS clusters; single-particle SERS sensitivity study; EIS spectra of the different layers on gold surface; schematic illustration for bioconjugation of SERS clusters with antibody, SERS detection for 350 at 0.1 pg/mL, and concentration-dependent response curve, specific study for 350 detection and sensitivity study for 030 detection, scheme for the fabrication of the microfluidic device. This material is available free of charge via the Internet at http://pubs.acs.org.

AUTHOR INFORMATION

Corresponding Authors

*E-mail: sebastian.schluecker@uni-due.de.
*E-mail: m.trau@uq.edu.au.

Notes

The authors declare no competing financial interest.

ACKNOWLEDGMENTS

This work was supported by the German Research Foundation (DFG, WA/3369-1), NIH Grant from USA (U01AIO82186-01), and ARC DECRA (DE120102503). We also would like to acknowledge the funding support from the National Breast Cancer Foundation of Australia to M.T. (CG-12-07). These grants have significantly contributed to the environment to stimulate the research described here. The fabrication work and Raman measurement was conducted at Queensland node of the Australian National Fabrication Facility (Q-ANFF).

REFERENCES

(1) Gold, L.; Ayers, D.; Bertino, J.; Bock, C.; Bock, A.; Brody, E. N.; Carter, J.; Dalby, A. B.; Eaton, B. E.; Fitzwater, T.; Flather, D.; Forbes, A.; Foreman, T.; Fowler, C.; Gawande, B.; Goss, M.; Gunn, M.; Gupta, S.; Halladay, D.; Heil, J.; Heilig, J.; Hicke, B.; Husar, G.; Janjic, N.; Jarvis, T.; Jennings, S.; Katilius, E.; Keeney, T. R.; Kim, N.; Koch, T. H.; Kraemer, S.; Kroiss, L.; Le, N.; Levine, D.; Lindsey, W.; Lollo, B.; Mayfield, W.; Mehan, M.; Mehler, R.; Nelson, S. K.; Nelson, M.; Nieuwlandt, D.; Nikrad, M.; Ochsner, U.; Ostroff, R. M.; Otis, M.; Parker, T.; Pietrasiewicz, S.; Resnicow, D. I.; Rohloff, J.; Sanders, G.; Sattin, S.; Schneider, D.; Singer, B.; Stanton, M.; Sterkel, A.; Stewart, A.; Stratford, S.; Vaught, J. D.; Vrkljan, M.; Walker, J. J.; Watrobka, M.; Waugh, S.; Weiss, A.; Wilcox, S. K.; Wolfson, A.; Wolk, S. K.; Zhang, C.; Zichi, D. *PLoS One* **2010**, *5*, No. e15004.
(2) Holliger, P.; Hudson, P. J. *Nat. Biotechnol.* **2005**, *23*, 1126−1136.
(3) Koide, A.; Koide, S. *Methods Mol. Biol.* **2012**, *911*, 431−443.
(4) Tillotson, B. J.; Cho, Y. K.; Shusta, E. V. *Methods* **2013**, *60*, 27−37.
(5) Ferrara, F.; Naranjo, L. A.; Kumar, S.; Gaiotto, T.; Mukundan, H.; Swanson, B.; Bradbury, A. R. *PLoS One* **2012**, *7*, No. e49535.
(6) Gray, S. A.; Weigel, K. M.; Ali, I. K. M.; Lakey, A. A.; Capalungan, J.; Domingo, G. J.; Cangelosi, G. A. *PLoS One* **2012**, *7*, No. e32042.
(7) Grewal, Y. S.; Shiddiky, M. J. A.; Gray, S. A.; Weigel, K. M.; Cangelosi, G. A.; Trau, M. *Chem. Commun.* **2013**, *49*, 1551−1553.
(8) Grewal, Y. S.; Shiddiky, M. J. A.; Spadafora, L. J.; Cangelosi, G. A.; Trau, M. *Biosens. Bioelectron.* **2014**, *55*, 417−422.
(9) Tanyuksel, M.; Petri, W. A. *Clin. Microbiol. Rev.* **2003**, *16*, 713−729.
(10) Haque, R.; Petri, W. A., Jr. *Arch. Med. Res.* **2006**, *37*, 273−276.
(11) Grubisha, D. S.; Lipert, R. J.; Park, H.-Y.; Driskell, J.; Porter, M. D. *Anal. Chem.* **2003**, *75*, 5936−5943.
(12) Faulds, K.; McKenzie, F.; Smith, W. E.; Graham, D. *Angew. Chem. Int. Ed.* **2007**, *46*, 1829−1833.
(13) Wang, G.; Park, H. Y.; Lipert, R. J.; Porter, M. D. *Anal. Chem.* **2009**, *81*, 9643−9650.
(14) Yang, J.; Palla, M.; Bosco, F. G.; Rindzevicius, T.; Alstrøm, T. S.; Schmidt, M. S.; Boisen, A.; Ju, J.; Lin, Q. *ACS Nano* **2013**, *7*, 5350−5359.
(15) Li, M.; Cushing, S. K.; Zhang, J.; Suri, S.; Evans, R.; Petros, W. P.; Gibson, L. F.; Ma, D.; Liu, Y.; Wu, N. *ACS Nano* **2013**, *7*, 4967−4976.
(16) Hatab, N. A.; Hsueh, C. H.; Gaddis, A. L.; Retterer, S. T.; Li, J. H.; Eres, G.; Zhang, Z.; Gu, B. *Nanolett.* **2010**, *10*, 4952−4955.
(17) Li, S.; Pedano, M. L.; Chang, S. H.; Mirkin, C. A.; Schatz, G. C. *Nanolett.* **2010**, *10*, 1722−1727.
(18) Lee, S. J.; Morrill, A. R.; Moskovits, M. *J. Am. Chem. Soc.* **2006**, *128*, 2200−2201.
(19) Jiang, J.; Bosnick, K.; Maillard, M.; Brus, L. *J. Phys. Chem. B* **2003**, *107*, 9964−9972.
(20) Steinigeweg, D.; Schütz, M.; Salehi, M.; Schlücker, S. *Small* **2011**, *7*, 2443−2448.
(21) Rocks, L.; Faulds, K.; Graham, D. *Chem. Commun.* **2011**, *47*, 4415−4417.
(22) Giljohann, D. A.; Mirkin, C. A. *Nature* **2009**, *462*, 461−464.
(23) Perrault, S. D.; Chan, W. C. W. *J. Am. Chem. Soc.* **2009**, *131*, 17042−17043.
(24) Stacy, R.; Begley, D. W.; Phan, I.; Staker, B. L.; Van Voorhis, W. C.; Varani, G.; Buchko, G. W.; Stewart, L. J.; Myler, P. J. *Acta Crystallogr., Sect. F: Struct. Biol. Cryst. Commun.* **2011**, *67*, 979−984.
(25) Bryan, C. M.; Bhandari, J.; Napuli, A. J.; Leibly, D. J.; Choi, R.; Kelley, A.; Van Voorhis, W. C.; Edwards, T. E.; Stewart, L. J. *Acta Crystallogr., Sect. F: Struct. Biol. Cryst. Commun.* **2011**, *67*, 1010−1014.
(26) Chao, G.; Lau, W. L.; Hackel, B. J.; Sazinsky, S. L.; Lippow, S. M.; Wittrup, K. D. *Nat. Protoc.* **2006**, *1*, 755−768.
(27) Ali, I. K.; Haque, R.; Siddique, A.; Kabir, M.; Sherman, N. E.; Gray, S. A.; Cangelosi, G. A.; Petri, W. A. *PLoS Neglected Trop. Dis.* **2012**, *6*, No. e1643.
(28) Ehrenkaufer, G. M.; Haque, R.; Hackney, J. A.; Eichinger, D. J.; Singh, U. *Cell. Microbiol.* **2007**, *9*, 1426−1444.
(29) Salehi, M.; Schneider, L.; Ströbel, P.; Marx, A.; Packeisen, J.; Schlücker, S. *Nanoscale.* **2014**, *6*, 2361−2367.
(30) Küstner, B.; Gellner, M.; Schütz, M.; Schöppler, F.; Marx, A.; Ströbel, P.; Adam, P.; Schmuck, C.; Schlücker, S. *Angew. Chem., Int. Ed* **2009**, *48*, 1950−1953.
(31) Jehn, C.; Küstner, B.; Adam, P.; Marx, A.; Ströbel, P.; Schmuck, C.; Schlücker, S. *Phys. Chem. Chem. Phys.* **2009**, *11*, 7499−7504.
(32) Orendorff, C. J.; Tapan, A. G.; Sau, K.; Murphy, C. J. *Anal. Chem.* **2005**, *77*, 3261−3266.
(33) Gellner, M.; Steinigeweg, D.; Ichilmann, S.; Salehi, M.; Schütz, M.; Kömpe, K.; Haase, M.; Schlücker, S. *Small* **2011**, *7*, 3445−3451.

(34) Salehi, M.; Steinigeweg, D.; Ströbel, P.; Marx, A.; Packeisen, J.; Schlücker, S. *J. Biophotonics* **2013**, *6*, 785−792.
(35) Wang, Y.; Salehi, M.; Schütz, M.; Rudi, K.; Schlücker, S. *Analyst* **2013**, *138*, 1764−1771.
(36) Wang, Y.; Salehi, M.; Schütz, M.; Schlücker, S. *Chem. Commun.* **2014**, *50*, 2711−2714.